

Nd-doped porous CeO₂ abrasives for chemical mechanical polishing of SiO₂ films

Yongyu Fan ^{a,b}, Jie Jiao ^{a,b}, Lang Zhao ^{a,*}, Jinkui Tang ^{a,b,**}, Chuandong Chen ^c, Na Fan ^c

^a State Key Laboratory of Rare Earth Resource Utilization, Changchun Institute of Applied Chemistry, Chinese Academy of Sciences, Changchun, Jilin, 130022, PR China

^b School of Applied Chemistry and Engineering, University of Science and Technology of China, Hefei, Anhui, 230026, PR China

^c Baotou Research Institute of Rare Earths, Inner Mongolia, 014030, PR China



ARTICLE INFO

Keywords:

Chemical mechanical polishing
Porous ceria
SiO₂ wafer
Doping

ABSTRACT

Chemical mechanical polishing (CMP) is a crucial step in integrated circuit manufacturing, and as chip feature sizes continue to shrink, there is an escalating demand for improved polishing performance. In this study, monodisperse porous CeO₂ nanospheres were synthesized and then modified through Nd doping. The structural and chemical characterization confirmed the enrichment effect on surface defects (Ce³⁺ and oxygen vacancies) due to the doping, with the percentage of Ce³⁺ in pCeO₂-Nd materials (39%) being higher than that of pCeO₂ (31%). Furthermore, for the CMP application on silicon wafers, the material removal rate (MRR) of pCeO₂-Nd reached 126.3 ± 17.5 nm/min, which is a 56% improvement over that of pCeO₂. In addition, the surface roughness (Ra) of the localized area ($3 \times 3 \mu\text{m}^2$) was reduced from initially 0.813 ± 0.02 nm to 0.296 ± 0.02 nm after polishing with pCeO₂. The chemical bonding of Ce–O–Si is considered to be the bridge between the structural characteristics of the abrasive and the polishing properties, whose presence makes the CMP process more efficient and high-quality.

1. Introduction

The semiconductor industry is expected to revitalize from the cyclical downturn with the rise of artificial intelligence, mega data, and other emerging digital industries, which also drives the development of chemical mechanical polishing (CMP), one of the key technologies in integrated circuit (IC) manufacturing [1–3]. Polishing materials significantly affect the capacity and quality of downstream chips. Among them, abrasives are responsible for transmitting mechanical energy and modifying chemical surfaces, whose structural characteristics directly affect the results of CMP.

CeO₂, as one of the mainstream abrasives, has a superior crystal structure and excellent tribocatalytic activity [4], resulting in a strong affinity for SiO₂, which facilitates the efficient removal of SiO₂ by the “Chemical Tooth” effect [5]. Based on the concept that structure determines properties, the researchers designed CeO₂-based core-shell abrasives with non-rigid mechanical properties using a material with low elastic modulus as the core [6–10]. Furthermore, the polishing properties were improved by ion doping [11–14] and other forms of

energy were introduced to develop new CMP techniques, such as photochemical mechanical polishing (PCMP) [11,13,15–17], electrochemical mechanical polishing (ECMP) [7,18], and magnetic-field-assisted polishing [19]. Since the crystallization temperature of TiO₂ is 450 °C, which is higher than the decomposition temperature (300 °C) of polystyrene (PS), it is impossible to synthesize PS/CeO₂–TiO₂ directly on the foundation of PS/CeO₂. In response, Gao [20] improved the preparation process, in which the CeO₂–TiO₂ composite particles were synthesized and then coated on the surface of PS. Yet, the morphological diversity and non-spherical shape of as-produced abrasives may limit widespread application. Chen [21] replaced the inorganic photocatalyst (TiO₂) with the organic material polyaniline (PANI) to obtain PS/PANI/CeO₂ abrasives. Not only addressed the preparation problem but also successfully constructed heterojunctions to achieve optimization of material removal rate by enhanced photocatalysis. Subsequently, they considered one material (carbon spheres, CS) to realize the actions of both PS and PANI components resulting in CS/CeO₂ core-shell abrasives [22]. The Carbon skeleton of CS provided additional charge transfer pathways, effectively extending the lifetime

* Corresponding author.

** Corresponding author. State Key Laboratory of Rare Earth Resource Utilization, Changchun Institute of Applied Chemistry, Chinese Academy of Sciences, Changchun, Jilin, 130022, PR China.

E-mail addresses: zhaolang@ciac.ac.cn (L. Zhao), tang@ciac.ac.cn (J. Tang).

of photogenerated charges for high-performance UV-assisted polishing. However, the synthesis procedure of core-shell abrasives is complicated and the shell layer is prone to breakage, causing serious contamination of the wafer surface. In this regard, Chen [23] directly synthesized cerium oxide abrasives with porous structure, which facilitate the polishing performance by optimizing interfacial contact behavior between abrasives and workpieces. Kim [24] synthesized ceria nanoparticles with different dopant concentrations of La and Nd, finding that the increase in electron density reduced the energy of oxygen vacancy formation when the low-oxidation state element replaces Ce⁴⁺.

In this work, monodisperse porous CeO₂ (pCeO₂) was synthesized by hydrothermal method and modified by Nd doping (pCeO₂-Nd). It's well known that the preparation of abrasives is the first step to achieving the desired polishing results. Compared to previous reports on doping modification, this work provided abrasives with better morphology consistency and excellent monodispersity, then explored the effect of doping amount on morphology as well as the heat treatment process. On the other hand, we construct a more direct link between the structural characterization of the material synthesis (Ce³⁺, V_O, etc.) and the mechanical/abrasive properties of the materials.

2. Materials and methods

2.1. Chemicals

The chemical reagents used in the experiments are as follows. Cerium nitrate (Ce(NO₃)₃·6H₂O, >98%), neodymium nitrate (Nd (NO₃)₃·6H₂O, >98%), and ethylene glycol were purchased from Shanghai MACKLIN Biochemical Co. Acetic acid (CH₃COOH) was provided by Xilong Scientific Co., Ltd. All chemicals were used without any further purification.

2.2. Synthesis of abrasives

Monodisperse CeO₂ mesoporous spheres were obtained via a reproducible and one-step synthetic strategy previously reported [25]. In a typical preparation, 1.5 g Ce(NO₃)₃·6H₂O was dissolved in 1.5 mL of Deionized water (DI) with 45 mL of ethylene glycol, and 1.5 mL of acetic acid (CH₃COOH) was added dropwise. After thorough stirring, the mixture was transferred to a polytetrafluoroethylene liner, heated at 180 °C for 240 min, then cooled to room temperature. Subsequently, the resultant precipitates were centrifuged at 12000 rpm for 10 min, washed with DI and ethanol, and dried at 80 °C for 12 h to obtain pCeO₂ precursor.

For comparison, pCeO₂-Nd precursors with varied Nd content were ready following a similar procedure as described above, with slight modifications. Identical to the previous synthesis except for the addition of Neodymium nitrate. Specifically, the doping amounts of 0.169, 0.156, 0.141, and 0.127. To investigate the impact of calcination temperature on the structural characteristics of abrasives, the above precursors were calcined at 300 °C, 400 °C, 500 °C, and 600 °C in a muffle furnace for 2 h, respectively.

2.3. Polishing tests

Substrates to be polished were cut into rectangular pieces of ca. 20 mm in length and ca. 15 mm in width. The slurries were made with pCeO₂ and pCeO₂-Nd treated by calcination at 600 °C, at a concentration of 1.0 wt%, moreover, a small amount of PVP (1.0 wt%) as a dispersant, and the pH of slurry was maintained at 10 using NaOH. Prior to use, the slurries must be thoroughly mixed and ultrasonically treated for 30 min. Polishing tests were conducted on Bruker Universal Mechanical Tester (UMT Tribolab). For each experimental run, the head/pad rotational speed was 120/90 rpm, the polishing pressure was 8 N, and the slurry was delivered to the surface of the polishing pad by peristaltic pump at a flow rate of 100 mL/min, and polishing time was 1 min. Subsequently,

the polished wafer was cleaned by sonication with DI, ethanol, and SC1 (NH₃·H₂O: H₂O₂: H₂O = 1 : 1 : 5) cleaning solution, then air-dried and stored at room temperature.

$$\text{MRR} = \frac{m_0 - m}{\rho \cdot S \cdot t} \quad (1)$$

The material removal rate (MRR, nm/min) was calculated by a weight-loss method as above [26], where wafer mass was weighed by ultra-precision electronic balance (XS105, Mettler Toledo, exact to 0.01 mg). Herein, m_0 and m (mg) are the masses before and after polishing, ρ (2.2 g/cm³) is the density of wafer, S (cm²) is the surface area of the polishing, and t (s) is the polishing time. Furthermore, the polishing efficiency and roughness data provided are the averages of three runs with standard deviation.

The high-resolution surface morphologies of wafers before and after polishing were characterized using atomic force microscopy (AFM, Nanoman VS, Bruker) with a scanning range of 3 × 3 μm² (256 pixels per line) in tapping mode. The recorded data were processed using the software (NanoScope Analysis) to determine the two-dimensional (2D)/three-dimensional (3D) images and the average roughness (Ra). In addition, for all AFM measurements, a commercial AFM probe (OLTESPA-R3) with a cantilever resonance frequency of 70 kHz, an elasticity factor of 2 N/m, and a tip radius of curvature of 7 nm was applied.

2.4. Characterization

As-synthesized particles were observed by field emission scanning electron microscopy (SEM, Hitachi S4800) equipped with energy dispersive spectroscopy (EDS) system and transmission electron microscopy (TEM, JEOL JEM-2010 EX). The crystal structures were characterized via powder X-ray diffractometer (XRD, Cu K α , λ = 1.4518 Å) over the 2θ ranging from 10° to 90°. Ultraviolet-visible diffuse reflectance spectroscopy (UV-vis DRS) was performed using Shimadzu UV-3600. The formation of oxygen vacancies was characterized using Raman spectroscopy (HORIBA T64000) in the test range of 400 nm–700 nm. X-ray photoelectron spectroscopy (XPS) was obtained by PHI-5000 Versaprobe III spectrometer with Al K α radiation ($h\nu$ = 1486.6 eV). Particle size distribution were examined by a Zetasizer Nano ZS (Malvern Instruments, UK).

3. Results and discussion

3.1. Structure and morphology analyses

Firstly, the appearance and dispersion of the designed abrasives were determined by SEM as shown in Fig. 1. The pCeO₂ and pCeO₂-Nd nano-abrasives obtained by hydrothermal method were monodisperse spheres with mixed particle sizes (80–180 nm). Comparing the samples with different Nd doping, the abrasives with loading of 0.141 (Fig. 1 b) had the most ideal morphology with intact spherical particles, keeping the basic morphology of the virgin pCeO₂. While excessive or insufficient quantities of doping had resulted in severe breakage of the nanospheres. Such abrasives may further fragment during polishing causing surface scratches, which significantly affect the polishing quality as well as pose a challenge to post-polishing cleaning. Therefore, pCeO₂-Nd with a doping amount of 0.141 was selected for the subsequent research.

Subsequently, thermogravimetric tests (Fig. 2) were carried out to obtain a suitable range of calcination temperatures for the precursors. The weight loss in the low-temperature range (below 150 °C) can be attributed to the removal of adsorbed water from porous CeO₂, and in the range from 150 °C to 400 °C corresponds to the removal of hydroxyl groups from hydroxides (formation of oxides) and the decomposition of residual organic matter, where the decomposition temperature of ethylene glycol is 215 °C. Above 600 °C the weight loss curve tends to level off and the mass is unchanged. Given above, the precursors were

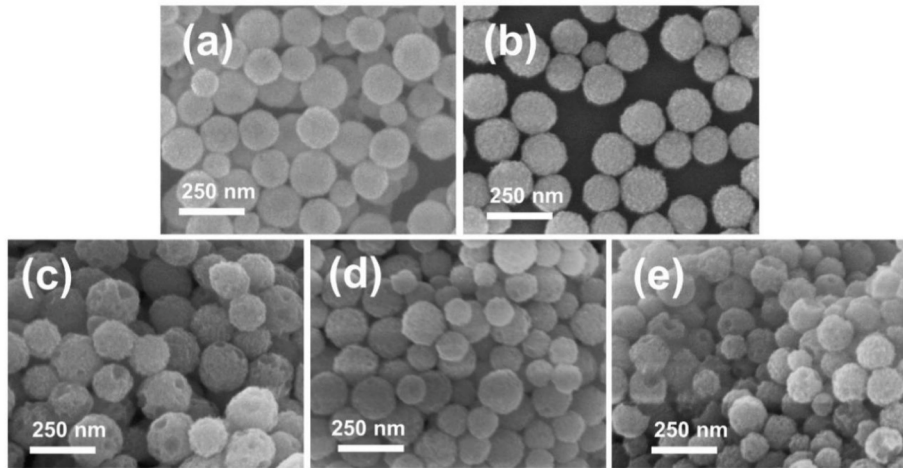


Fig. 1. SEM of (a) pCeO₂ and pCeO₂-Nd with different doping ratios: (b) 0.141, (c) 0.169, (d) 0.156, and (e) 0.127.

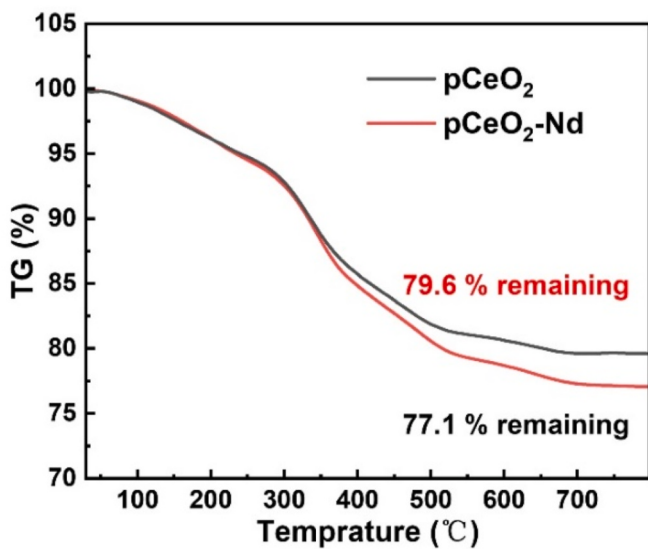


Fig. 2. Thermogravimetric curves of pCeO₂ and pCeO₂-Nd abrasives.

calcined at 300 °C, 400 °C, 500 °C and 600 °C, respectively, to examine the dependency of calcination temperature on sample structure.

The above series of materials were characterised by XRD to find the optimal calcination process. In Fig. 3, the peaks located at ca. 28.6°, 33.1°, 47.0°, and 56.3° can be indexed to lattice planes of (111), (200),

(220), (311), and (331) reflections of cubic fluorite-type CeO₂ (JCPDS No. 34-0394) [27]. As calcination temperature increases, the full width at half maximum (FWHM) of CeO₂ decreased and the peaks got sharper, implying superior crystallinity. According to Bragg's equation and the Scherrer formula [28], the calculated data based on the (111) XRD diffractions were shown in Table 1. Compared to pCeO₂, the interplanar spacing of pCeO₂-Nd obtained at the same calcination temperature was all increased. In particular, the interplanar spacing of pCeO₂-Nd calcined at 600 °C was 3.126 Å, which was slightly larger than that of pCeO₂ (3.122 Å). The ionic radius of Nd³⁺ is about 99.5 pm compared to 92.0 pm for Ce⁴⁺, hence lattice expansion was expected due to the incorporation of Nd³⁺ [24,29]. Moreover, pCeO₂ and pCeO₂-Nd nanocrystal sizes calculated from the Scherrer formula were 6.318 nm and 6.496 nm,

Table 1
Properties of the Ceria-based composite particles by XRD.

| Lattice | Calcine temperature (°C) | 2 Theta | FWHM | Crystal spacing (Å) | Lattice constant (Å) | Average grain size (nm) |
|-----------------------|--------------------------|---------|-------|---------------------|----------------------|-------------------------|
| pCeO ₂ | 300 | 28.64 | 1.950 | 3.114 | 5.393 | 4.156 |
| | 400 | 28.52 | 1.871 | 3.126 | 5.414 | 4.330 |
| | 500 | 28.62 | 1.729 | 3.115 | 5.395 | 4.687 |
| | 600 | 28.56 | 1.283 | 3.122 | 5.407 | 6.318 |
| pCeO ₂ -Nd | 300 | 28.44 | 2.203 | 3.134 | 5.428 | 3.678 |
| | 400 | 28.49 | 2.034 | 3.129 | 5.419 | 3.983 |
| | 500 | 28.44 | 1.697 | 3.135 | 5.429 | 4.775 |
| | 600 | 28.52 | 1.248 | 3.126 | 5.414 | 6.491 |
| <hr/> | | | | | | |

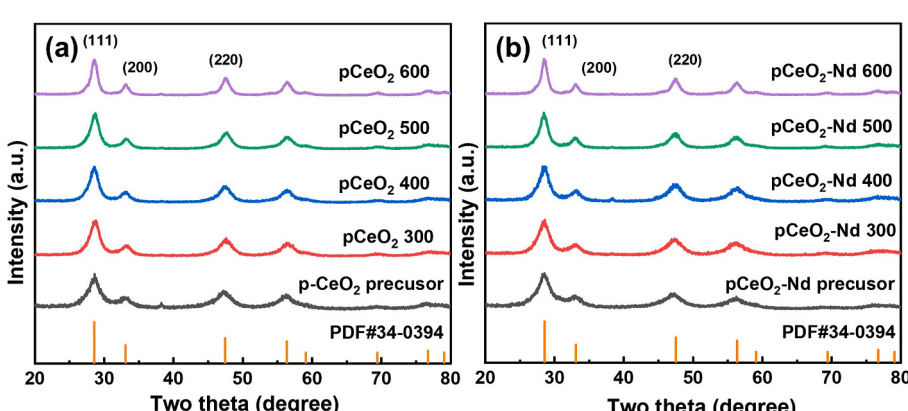


Fig. 3. XRD images of precursor and calcined samples: (a) pCeO₂, (b) pCeO₂-Nd.

respectively. To sum up, the samples calcined at 600 °C with optimum crystallinity were finally selected for subsequent characterization.

$$2d \sin \theta = n\lambda \quad (2)$$

$$D = K\lambda / (\beta \cos \theta) \quad (3)$$

Here, d is interplanar spacing, θ is the angle between the incident X-rays and the corresponding crystal plane, λ is the X-ray wavelength ($\lambda = 0.15406$ nm), n is the number of diffraction levels, D is average grain size, β is FWHM, and K is a constant related to crystal shape, taken as 0.89 in this work [30].

Following the discussion of the doping amount and the calcination process, the internal structure of the screened abrasive was observed by TEM and EDS to recognize whether it meets the design. As seen in Fig. 4, the porous materials were stacked by CeO₂ particles with a size of about 5 nm, hence revealing irregular pore structures inside abrasives. In contrast to pCeO₂, the doped CeO₂ particles appeared denser, causing the pore size narrower in pCeO₂-Nd. In the high-resolution TEM, clear and uniform CeO₂ lattice stripes were observed, and (111) interplanar spacing expanded from 0.323 nm to 0.375 nm after modification, signifying the expansion of the CeO₂ lattice, which is consistent with the XRD analysis. EDS-Mapping analysis can visually reflect the element distribution on the spherical abrasives. Fig. 4 (c) revealed that elements of Ce, O, and Nd were uniformly distributed on the pCeO₂-Nd nanospheres, which also revealed the successful doping of Nd ions.

Later, the porous structure of the abrasive was confirmed by the nitrogen adsorption-desorption isotherms in Fig. 5. The specific surface areas of pCeO₂ and pCeO₂-Nd were 143.5 m²/g and 98.49 m²/g. Based on the adsorption-branched data, the average pore sizes of pCeO₂ and pCeO₂-Nd were 5.665 nm and 1.927 nm, respectively, according to the Barrett-Joiner-Halenda (BJH) calculations. The doping modification resulted in a denser structure of the porous abrasive, which is consistent with the TEM results.

Once the basic structure of the synthesized material has been clarified, it is necessary to characterize the surface defects of CeO₂ particles induced by doping. UV-Vis diffuse reflectance spectra of the proposed products were shown in Fig. 6, the distinct peaks located at 250–350 nm possibly revealed the electron transition from O 2p to Ce 4f orbital. The absorption edges of pCeO₂ and pCeO₂-Nd. were ca. 403 nm and 415 nm, respectively. In other words, a pronounced redshift (shift to higher wavelengths) can be detected for the pCeO₂-Nd, which may be owing to the lattice defects caused by Nd-doping. Considering the band gap energy (E_g) of abrasives, the Schuster-Kubelka-Munk [31] absorption function (ahv) versus the photon energy (hv) was plotted according to Eq. (4).

(ahv)ⁿ = $A(hv - E_g)$ (4)

Here, α is the absorption coefficient, hv is the photon energy, A is the proportionality constant, and n is taken as 2 (CeO₂ is a direct gap semiconductor). The results were shown in Fig. 6 (b), and the approximate band gap can be identified from the horizontal axis intercept. For pCeO₂ and pCeO₂-Nd, the E_g were 3.28 eV and 3.16 eV, respectively. The narrowed band gap could be explained by the formation of doping transition states, derived from the increase in surface defects, which imply that the pCeO₂-Nd possesses high Ce³⁺ and V_O concentrations compared to the pCeO₂. Subsequently, Raman and XPS were applied for further identification of CeO₂ surface defects.

Moreover, Raman spectrum is a nondestructive technique applied to detect oxygen vacancy defects in CeO₂. In Fig. 7, the strong peaks at ca. 460 cm⁻¹ can be ascribed to the typical Raman vibration mode (F_{2g}) of the cubic fluorite-type CeO₂ materials [22]. In addition, the weak peak at 600 cm⁻¹ was also assigned to structural defects of CeO₂ (typically V_O) resulting from doping modification [32]. Hence, the peak intensity ratio of the band at 600 cm⁻¹ to 460 cm⁻¹ (I_{600}/I_{460}) could reflect the concentration of V_O in CeO₂ [23,33]. The calculated I_{600}/I_{460} value for pCeO₂-Nd (ca. 0.10) was higher than that of pCeO₂ (ca. 0.04), a preliminary indication of the increase in V_O concentration after Nd doping.

To accurately identify the surface chemical composition and

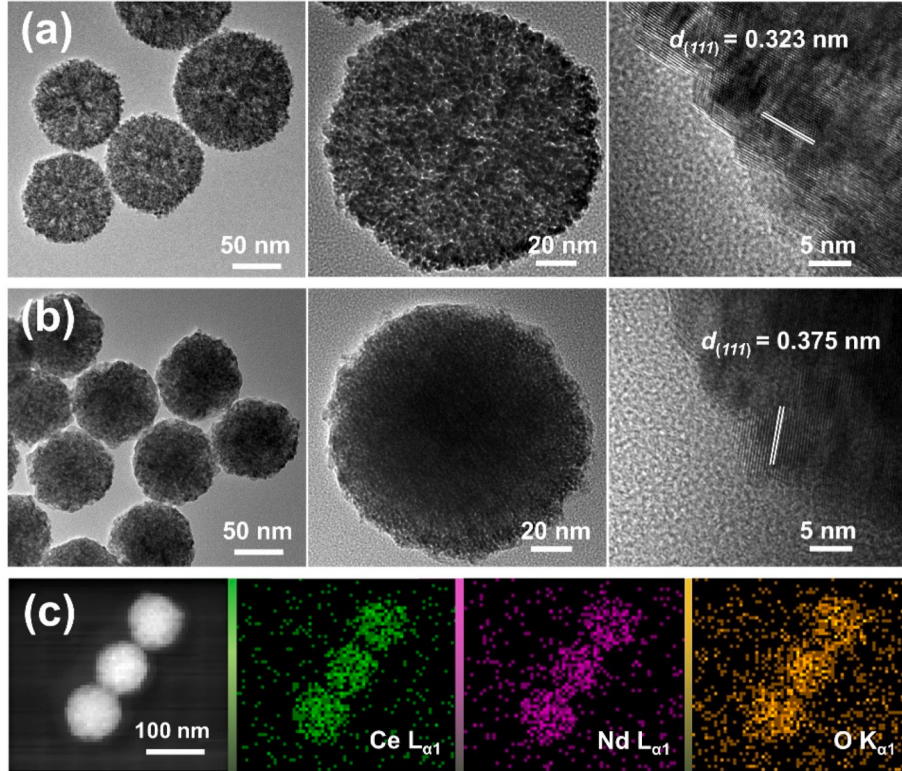


Fig. 4. TEM images of the materials obtained by calcination at 600 °C: (a) pCeO₂ and (b) pCeO₂-Nd; (c) EDS mapping of pCeO₂-Nd.

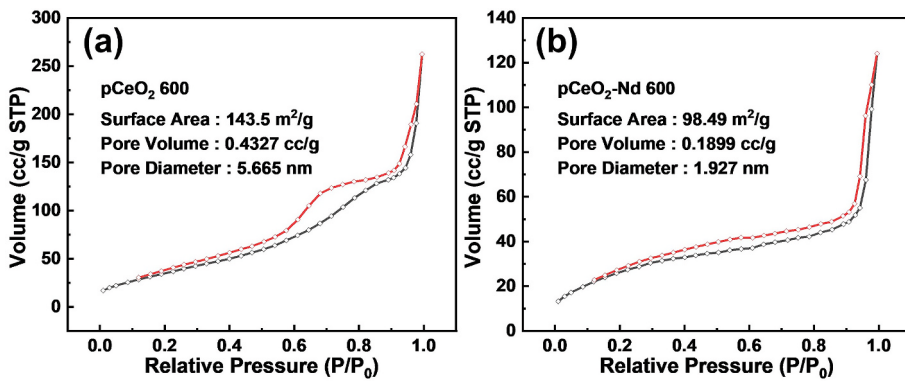


Fig. 5. N₂ adsorption/desorption isotherms of (a) pCeO₂ and (b) pCeO₂-Nd.

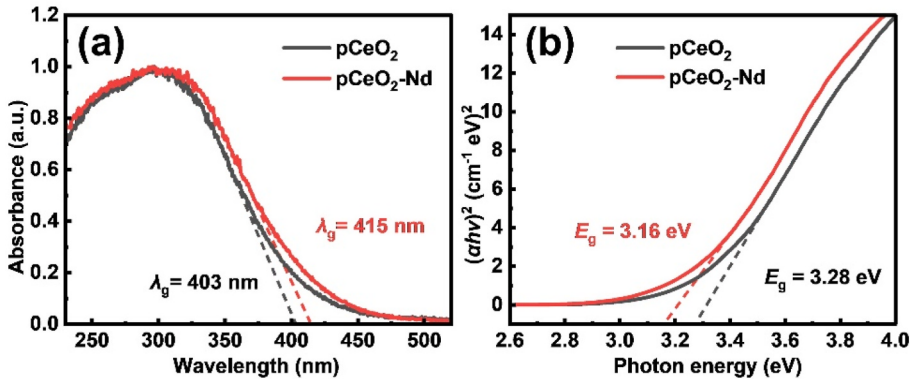


Fig. 6. (a) UV-vis diffuse reflectance spectra and (b) the corresponding Tauc plots.

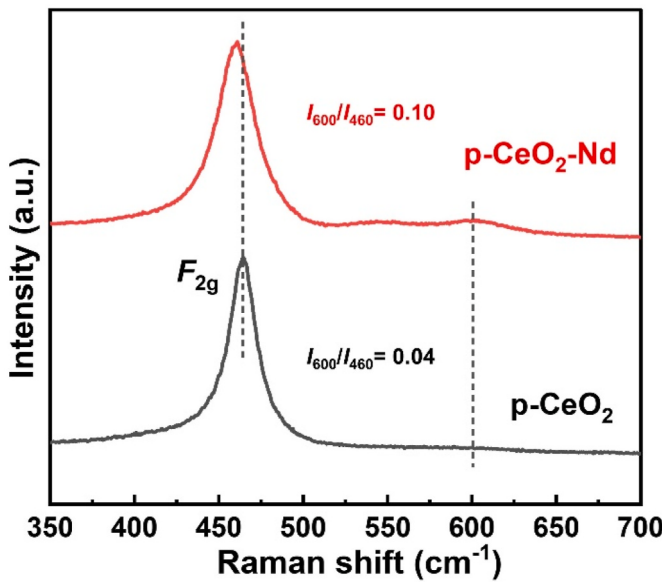


Fig. 7. Raman spectra of pCeO₂ and pCeO₂-Nd.

elemental valence states of the materials, pCeO₂ and pCeO₂-Nd abrasives were analyzed by XPS spectroscopy. As seen in Fig. 8 (b), the peaks at ca. 982.3 eV and 1005.8 eV for pCeO₂-Nd, corresponding to Nd 3d_{3/2} and Nd 3d_{5/2}, respectively, proved the successful doping of Nd³⁺ ions. Fig. 9 (c) depicted the Ce 3d core level and two group peaks (denoted as v and u) obtained after deconvolution treatment, which suggests both valences (Ce³⁺ and Ce⁴⁺) are present in abrasives. Furthermore, the

ratio of the valence states of cerium can be determined semi-quantitatively using the combined peak areas of the respective valence states. The results obtained according to Eqs. (5)–(7) [22,33] were summarized in Table 2, where C and A represent concentration and area. The Ce³⁺ for pCeO₂-Nd was calculated to be 39%, while the value was only 31% in pCeO₂, indicating that Nd doping contributes to the increase of Ce³⁺ proportion on the surface of CeO₂.

Besides, the density of oxygen vacancy in CeO₂ abrasives can be inferred from the O 1s spectra, which are deconvoluted into three peaks, as illustrated in Fig. 9 (d). Peaks at about 529 eV, 531 eV, and 533 eV belonged to lattice oxygen (O α), surface oxygen (O β), and adsorbed oxygen (O γ), respectively. Where O α represents the O²⁻ ion in the CeO₂ lattice, O β (O²⁻, O₂²⁻ or O⁻) implies the existence of V_O in the CeO₂ substrate, and O γ are other weakly bound oxygen species, such as carbonate (CO₃²⁻), adsorbed molecular water and hydroxyl (OH⁻) [34]. The density of V_O can be calculated by the relation O β /(O α +O β +O γ) based on their peak areas, which ratio is 43.9% for pCeO₂ and 58.3% for pCeO₂-Nd (more oxygen vacancies), such trend is consistent with the Raman analysis.

In summary, Raman and XPS analyses directly evidenced the formation of V_O and the conversion of Ce⁴⁺ to Ce³⁺ due to Nd doping, which also provided a convincing basis for the apparent connection between the structural characterization (Ce³⁺, V_O, etc.) and the CMP performance of abrasives.

$$C(\text{Ce}^{3+}) = \frac{A(\text{Ce}^{3+})}{A(\text{Ce}^{3+}) + A(\text{Ce}^{4+})} \quad (5)$$

$$A(\text{Ce}^{3+}) = A(v_0) + A(v') + A(u_0) + A(u') \quad (6)$$

$$A(\text{Ce}^{4+}) = A(v) + A(v'') + A(v''') + A(u) + A(u'') + A(u''') \quad (7)$$

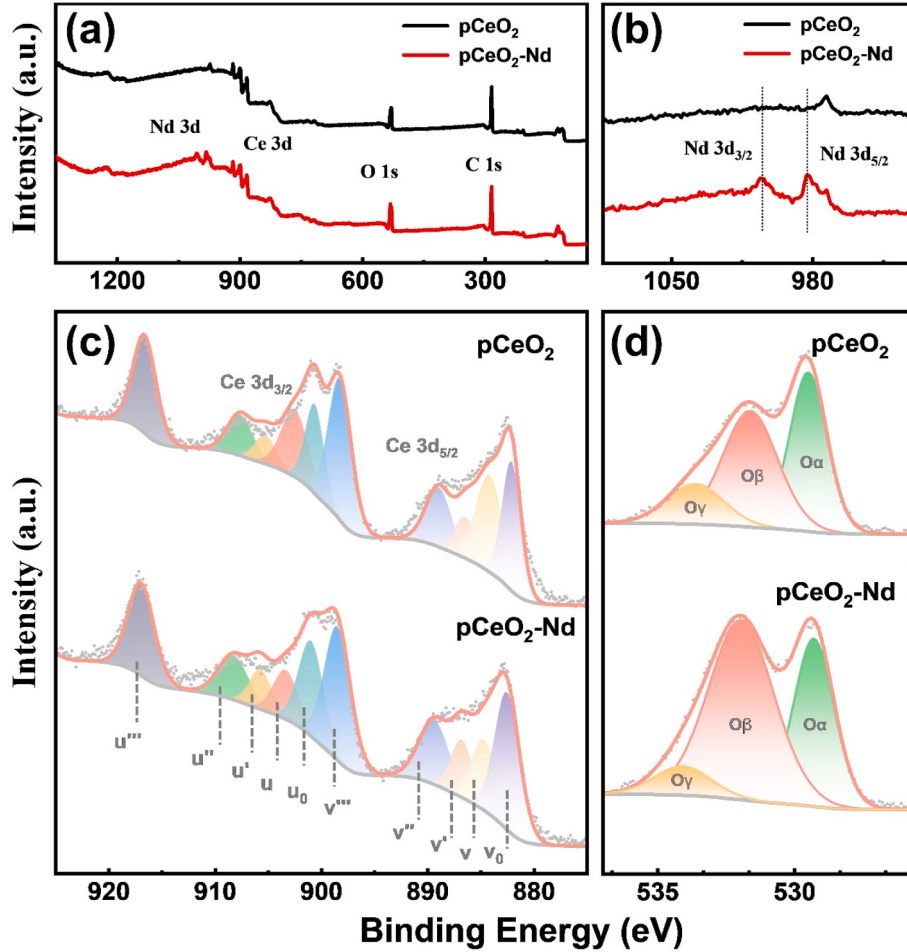


Fig. 8. XPS spectra results of pCeO₂ and pCeO₂-Nd: (a) full survey spectrum, (b) Nd 3d, (c) Ce 3d core level spectra, and (c) O1s core level spectra.

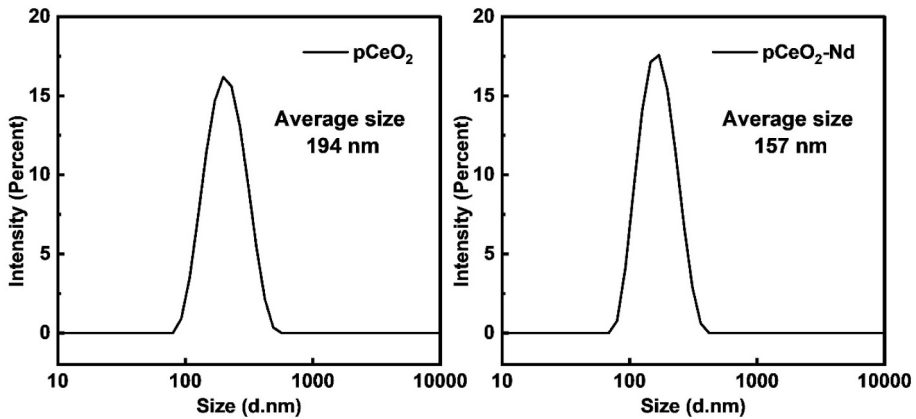


Fig. 9. Size distribution curve of pCeO₂ and pCeO₂-Nd.

3.2. CMP performances

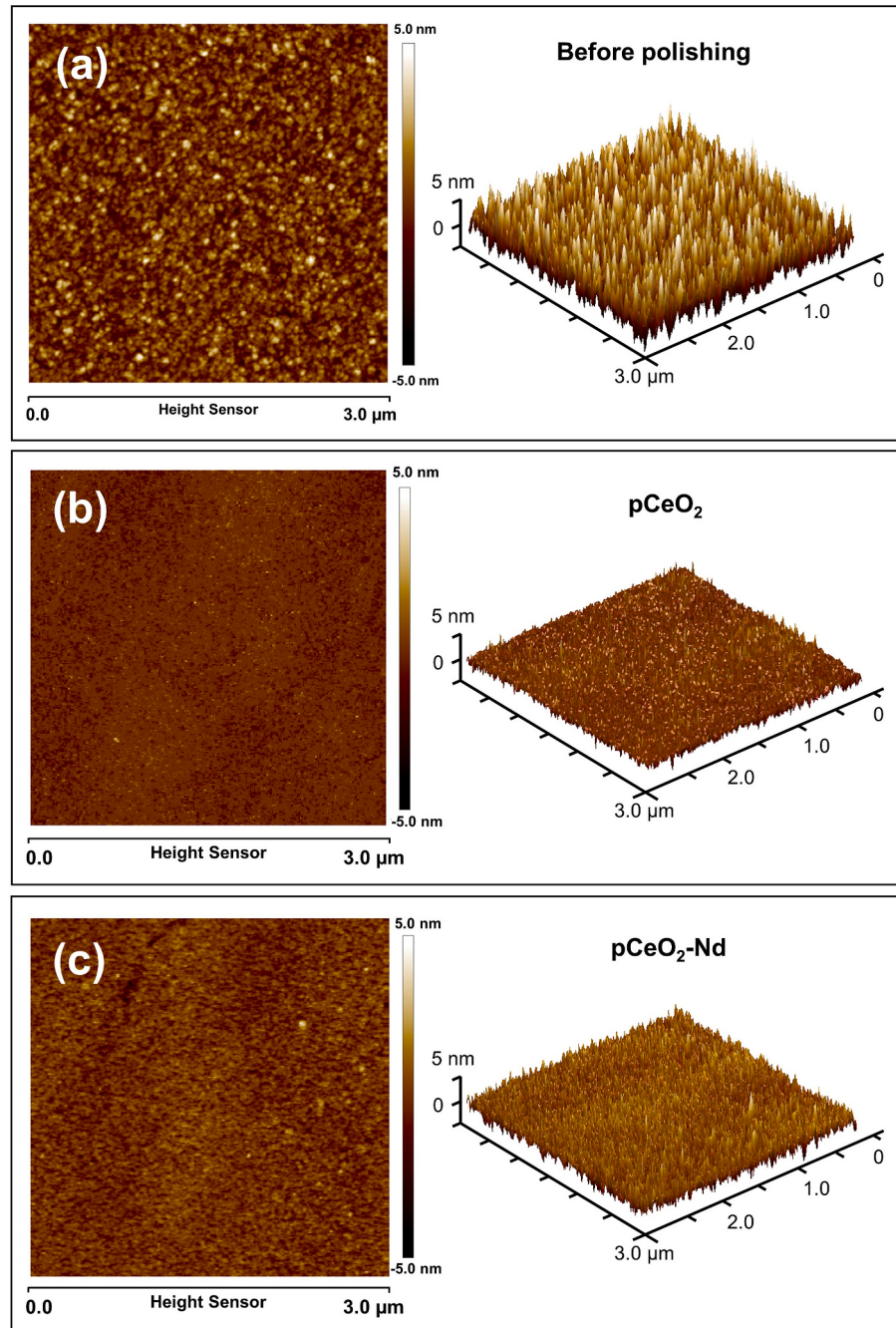
So far, the basic structure and surface defects of the abrasive have been identified, prior to polishing, the dispersion of the abrasive in the slurry needs to be considered. The results of particle size distribution based on the dynamic light scattering (DLS) method are shown in Fig. 9, the size of the abrasive is almost uniform, with an average size of 194 nm for pCeO₂-Nd and pCeO₂ of 157 nm, respectively, and there is no serious agglomeration.

Subsequently, we applied these highly dispersible polishing slurries to polishing tests. The 2D/3D morphology and surface roughness of the wafer surface were characterized by AFM. Fig. 10 (a) presented the wafer surface before polishing, which showed a non-uniform color distribution in 2D-AFM, and the 3D-AFM also clearly reflected a large number of nanoscale roughness peaks, which implies a relatively rough original surface. Besides, the Rain the range of $3 \times 3 \mu\text{m}^2$ was as high as $0.813 \pm 0.02 \text{ nm}$. Fig. 10 (b-c) illustrated the results after polishing by pCeO₂ and pCeO₂-Nd. Compared with the original surface, most of the nano-sized rough peaks in 3D-AFM have been removed, and the surface

Table 2

The oxidation states, the binding energies, and the peak areas of Ce species.

| | Ce ³⁺ v ₀ | v' | u ₀ | u' | Ce ⁴⁺ v | v'' | v''' | u | u'' | u''' | Ce ³⁺ content |
|-----------------------|------------------------------------|-------|----------------|-------|-----------------------|-------|-------|-------|-------|-------|--------------------------|
| pCeO ₂ | | | | | | | | | | | |
| BE (eV) | 882.1 | 886.5 | 900.6 | 905.3 | 884.2 | 889.0 | 898.3 | 902.5 | 907.7 | 916.6 | |
| Area | 24587 | 8904 | 17026 | 6166 | 26654 | 15638 | 33438 | 18457 | 10829 | 23154 | 31% |
| pCeO ₂ -Nd | | | | | | | | | | | |
| BE (eV) | 882.5 | 886.8 | 901.0 | 905.8 | 884.7 | 889.4 | 898.5 | 903.4 | 908.3 | 917.0 | |
| Area | 35134 | 12849 | 24329 | 8898 | 18145 | 19823 | 35960 | 12564 | 13727 | 24901 | 39% |

**Fig. 10.** AFM images of the surface (a) before polishing and after CMP with (b) pCeO₂ and (c) pCeO₂-Nd abrasives.

flatness of the wafer significantly improved. Especially, the Ra of the wafer surface was reduced to 0.296 ± 0.02 nm after polishing by pCeO₂, with the obtained MRR, another key evaluation index for polishing

performance, reaching 80.8 ± 8.7 nm/min. In the case of the doped-modified abrasive, the MRR was further increased to 126.3 ± 17.5 nm/min, an improvement of nearly 56%. However, the quality of the

polishing was not satisfactory, and the surface roughness was reduced only to 0.542 ± 0.03 nm. In response to the above results (Table 3), Firstly, MRR and surface roughness are a pair of contradictions, implying that the increase of MRR will cause a decrease of polishing quality to a certain extent. That is why adjusting the factors to realize the balance between them is a priority issue in the future. Secondly, compared to pCeO₂, the size of pCeO₂-Nd is reduced, possessing a larger surface area, and an increased proportion of Ce³⁺, contributing to a higher surface density of -OH groups through H₂O dissociation, which may further lead to more Ce-O-Si bonding. On the one hand, it can improve the MRR, nonetheless, making it challenging to remove ceria particles from the oxide surface after the CMP process. The residual abrasives will seriously affect the surface flatness, which is manifested in the rise of the roughness.

In conclusion, the porous cerium oxide abrasive is capable of CMP flattening, further research is still desired to optimize the abrasive properties, slurry formulation, and polishing process to obtain a higher-quality surface.

In order to ensure the designed porous abrasive will not break under the current polishing pressure, which will affect the polishing effect and post-cleaning, the polishing waste slurry was analyzed by SEM (see Fig. 11), revealing no significant change in abrasive morphology and particle size after use, affirming that the synthesized abrasive which possessed excellent structural stability.

3.3. CMP mechanism analysis

As stated above, the excellent morphology and high dispersion of the designed abrasive were verified by SEM and TEM, as well as the surface defects of CeO₂ particles were demonstrated by Raman, XPS, and DRS, finally, relatively improved polishing results were obtained in the CMP of wafers. Combined with previous reports, the bridge between the structural characteristics of the abrasive and the mechanical/abrasive properties is considered to be the Ce-O-Si chemical bonding. The surface defects of CeO₂ particles (especially Ce³⁺) facilitate the formation of Ce-O-Si at the interface between the abrasive and SiO₂ wafers, and the mechanism of material removal of SiO₂ is essentially related to the dynamic formation and breakage of Ce-O-Si bonds [11,35,36], whose presence makes the CMP process more productive and high-quality.

As early as 2001, Hoshino [37] discussed the formation of Ce-O-Si between abrasive and substrate by FT-IR-ATR. There are two peaks near 1100 cm, which are split into two peaks from one peak by polarised light, belonging to the asymmetric stretching mode. The splitting width was changed by polishing, indicating that the surface was modified by CeO₂. Inspired by this method, the surface of the wafer before and after polishing was analyzed, shown in Fig. 12, and the two peaks mentioned above do move after polishing, which is most likely due to the formation of Ce-O-Si. In addition, Miyamoto [38] applied the tight-binding quantum chemical molecular dynamics method to the investigations on the mechano-chemical reaction dynamics during the CMP process of SiO₂ surface by CeO₂ particles, suggesting that mechanical forces introduced by CeO₂ particles accelerate the chemical reactions at the CeO₂-SiO₂ interface, forming new Sisio₂-O_{CeO2}. Han [39] explored the adhesion mechanisms of ceria to the oxide surface, hypothesizing that chemical bonding of Ce-O-Si dominates under polishing conditions, leading to higher contamination at higher pH. Later, the strong additional peaks associated with Ce-O-Si bonding were detected in the O 1s

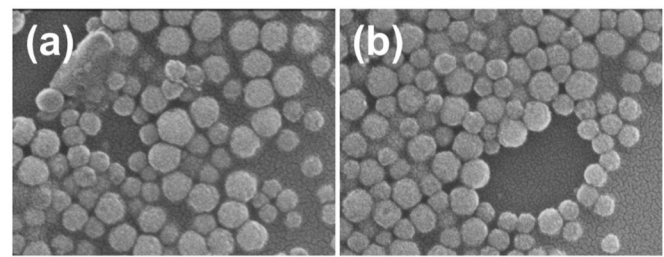


Fig. 11. SEM of the abrasives in waste slurries: (a) pCeO₂ and (b) pCeO₂-Nd.

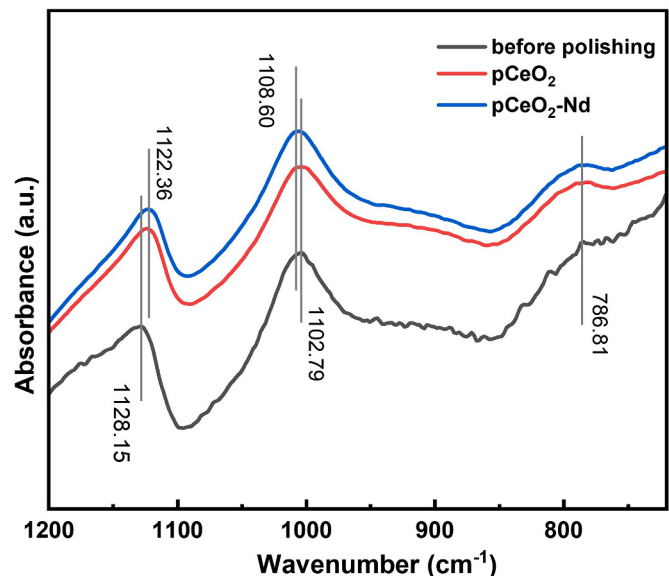


Fig. 12. IR of wafer surface before and after polishing with pCeO₂ and pCeO₂-Nd.

XPS spectra at binding energies of about 532 eV for surfaces polished at pH 8, validating the presence of Ce-O-Si bonding. Kim [24] confirmed the improved reactivities of the particles by doping by measuring the reduction of the work function of the doped ceria nanoparticles and the increase in the adhesion force with SiO₂.

In this work, the possible polishing mechanism is illustrated in Fig. 13. In the weakly alkaline polishing slurry, SiO₂ is chemically etched to form a surface soft layer prone to be removed, and numerous Si-O⁻ sites are generated on the SiO₂ surface. Alternatively, the V_O on the CeO₂ surface can react with water to form surface hydroxyl groups, which in turn react with the Si-O⁻ sites to form Ce-O-Si bonds (Reaction 8). Subsequently, the comparatively weak Si-O-Si bonds break under the mechanical action of the abrasives and polishing pad, allowing the SiO₂ soft layer to be removed in the form of lumps, which is the "lump removal model" proposed by Hoshino [37]. Furthermore, porous nanoparticles can effectively optimize the contact pattern between the abrasive and the wafer to reduce scratch damage [33], while increased contact area also benefits the polishing rate.



Since surface defects such as Ce³⁺ and V_O in CeO₂ abrasives could facilitate the frictional chemical activity and chemical bonding between CeO₂-SiO₂ [13,14], which accelerates the formation and breakage of Ce-O-Si bonds and ultimately improves the material removal rate of CMP. Compared to undoped abrasives, the nearly 56% increase in the polishing rate of pCeO₂-Nd can be attributed to the formation of doped transition states as demonstrated by DRS, which is essentially an enrichment effect of the doping modification on CeO₂ surface defects

Table 3
Results of polishing experiments.

| | Initial surface | CMP | |
|--------------|------------------|-------------------|-----------------------|
| | | pCeO ₂ | pCeO ₂ -Nd |
| MRR (nm/min) | – | 80.8 ± 8.7 | 126.3 ± 17.5 |
| Ra (nm) | 0.813 ± 0.02 | 0.296 ± 0.02 | 0.542 ± 0.03 |

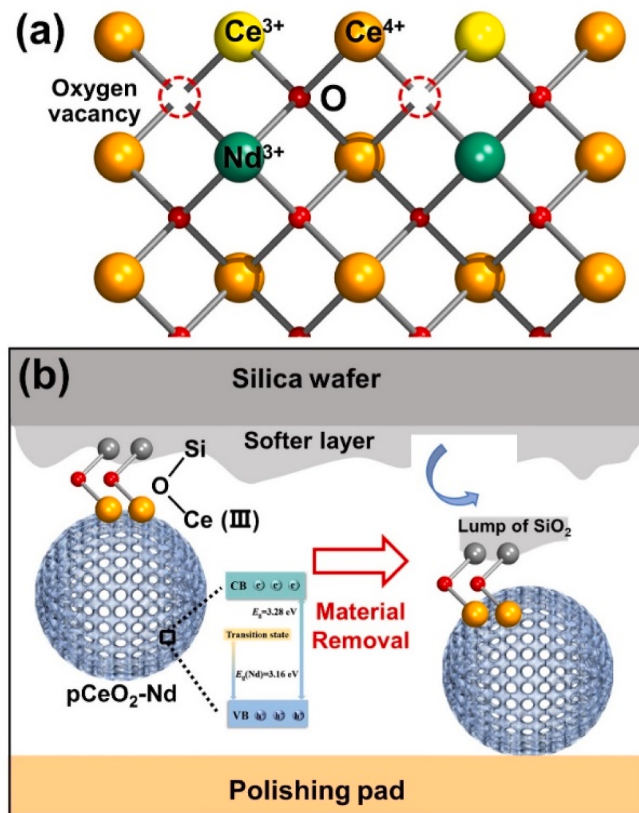


Fig. 13. (a) The atomic structure of Nd-doped CeO₂ surfaces, (b) Schematic of polishing mechanism.

[23]. As shown in Fig. 13 (a), the surface-exposed Ce⁴⁺ is replaced by Nd³⁺, and to achieve the electric equilibrium of the crystal, part of Ce⁴⁺ is converted to Ce³⁺ [13], which is accompanied by the formation of oxygen vacancies. Since lattice contraction due to the oxygen vacancies can be compensated by lattice expansion induced by ionic doping, the system also achieves stress balance. In summary, Nd doping can increase the number of defects on the CeO₂ surface to achieve charge and stress balance [40], and increased surface defects ultimately enhance polishing performance according to the polishing mechanism described above.

4. Conclusion

Porous cerium oxide nanospheres pCeO₂ with a particle size of 80–180 nm were synthesized by a hydrothermal method, which possesses excellent topographic consistency and excellent dispersibility. Subsequently, ionic doping and heat treatment processes were investigated, in which abrasives with doping amounts of 0.141 and calcination at 600 °C showed optimal sphericity and crystallinity. Raman spectra demonstrated ratios of I₆₀₀/I₄₆₀ for pCeO₂ and pCeO₂-Nd are 0.04 and 0.10, respectively. XPS indicated the proportion of Ce³⁺ in the pCeO₂-Nd material was 39%, higher than that of pCeO₂ (31%), implying an increase in V_O and Ce³⁺ due to doping. The chemical bonding of Ce–O–Si is considered to be the bridge between the structural characteristics of the abrasive and the mechanical/wear resistance properties, whose presence makes the CMP process more efficient and high-quality. Therefore, the MRR of pCeO₂-Nd was increased by nearly 56% compared to that of pCeO₂, reaching 126.3 ± 17.5 nm/min. The enhanced polishing rate may be associated with the increased surface defects and frictional chemical activity of doped abrasives. And the wafer roughness can be reduced from 0.813 nm to 0.296 nm after polishing with pCeO₂. This work identifies suitable doping and calcination processes and provides a practical program for the preparation and modification of porous CeO₂

abrasives.

CRediT authorship contribution statement

Yongyu Fan: Writing – original draft, Investigation, Formal analysis, Data curation. **Jie Jiao:** Data curation. **Lang Zhao:** Writing – review & editing, Funding acquisition, Data curation. **Jinkui Tang:** Supervision. **Chuandong Chen:** Software. **Na Fan:** Software.

Declaration of competing Interest

We confirm that this manuscript has not been published elsewhere and is not being considered elsewhere. All co-authors have contributed to the work, seen and agreed with the contents of the manuscript. The authors have no conflicts of interest.

Data availability

No data was used for the research described in the article.

Acknowledgments

This work was financially supported by Jilin Province Science and Technology Development Program (Grants YDZJ202201ZYTS518 and YDZJ202303CGZH002) and Special science and technology project of Northern rare earth (BFXT-2022-D-0021 and BFXT-2023-D-0014).

References

- [1] P.Z. Liu, Y. Nam, S.H. Lee, E. Kim, S. Jeon, K. Park, S.K. Hong, T. Kim, The mechanical effect of soft pad on copper chemical mechanical polishing, Mater. Sci. Semicond. Process. 155 (2023) 107256, <https://doi.org/10.1016/j.mssp.2022.107256>.
- [2] L. Jiang, Q. Li, Y. Chen, Y. Wu, M. Sun, L. Qian, Polyacrylic acid as a lubricant and a complement to 1,2,4-triazole for copper chemical mechanical polishing, Tribol. Lett. 71 (2023) 62, <https://doi.org/10.1007/s11249-023-01732-5>.
- [3] P. Zhang, G. Chen, Z. Ni, Y. Wang, K. Teng, S. Qian, D. Bian, Y. Zhao, The effect of Cu²⁺ ions and Glycine complex on chemical mechanical polishing (CMP) performance of SiC substrates, Tribol. Lett. 69 (2021) 94, <https://doi.org/10.1007/s11249-021-01468-0>.
- [4] J. Seo, A review on chemical and mechanical phenomena at the wafer interface during chemical mechanical planarization, J. Mater. Res. 36 (2021) 235–257, <https://doi.org/10.1557/s43578-020-00060-x>.
- [5] L.M. Cook, Chemical processes in glass polishing, J. Non-Cryst. Solids 120 (1990) 152–171, [https://doi.org/10.1016/0022-3093\(90\)90200-6](https://doi.org/10.1016/0022-3093(90)90200-6).
- [6] M. Wang, Z. Mu, T. Wang, Y. Chen, A. Chen, Double-layered core-shell heterostructures of mSiO₂@CdS@CeO₂ abrasives systems toward photochemical mechanical polishing (PCMP) applications, Appl. Surf. Sci. 614 (2023) 156274, <https://doi.org/10.1016/j.apsusc.2022.156274>.
- [7] B. Gao, W.J. Zhai, Q. Zhai, Y.Q. Shi, Polystyrene/CeO₂ core/shell abrasives for high-quality 4H-SiC surface in CMP: the effects of shell thickness, ECS J. Solid State Sci. Technol. 9 (2020) 044005, <https://doi.org/10.1149/2162-8777/ab871>.
- [8] Y. Chen, X. Ma, W. Cai, A. Chen, Preparation of three-dimensional dendritic-like mesoporous silica particles and their pore size-dependent polishing behavior and mechanism, J. Porous Mater. 26 (2019) 1869–1877, <https://doi.org/10.1007/s10934-019-00777-z>.
- [9] A. Chen, J. Long, Z. Li, Y. Chen, Dependency of structural change and polishing efficiency of meso-silica/ceria core/shell composite abrasives on calcination temperatures, J. Mater. Sci. Mater. Electron. 29 (2018) 11466–11477, <https://doi.org/10.1007/s10854-018-9239-1>.
- [10] Y. Chen, R.W. Long, Polishing behavior of PS/CeO₂ hybrid microspheres with controlled shell thickness on silicon dioxide CMP, Appl. Surf. Sci. 257 (2011) 8679–8685, <https://doi.org/10.1016/j.apsusc.2011.05.047>.
- [11] H. Doi, M. Suzuki, K. Kinuta, Effects of Ce³⁺ on removal rate of ceria slurries, in: Chemical Mechanical Polishing for SiO₂, IEEE, Kobe, Japan, 2014.
- [12] N.-Y. Kim, G. Kim, H. Sun, U. Hwang, J. Kim, D. Kwak, I.-K. Park, T. Kim, J. Suhr, J.-D. Nam, A nanoclustered ceria abrasives with low crystallinity and high Ce³⁺/Ce⁴⁺ ratio for scratch reduction and high oxide removal rates in the chemical mechanical planarization, J. Mater. Sci. 57 (2022) 12318–12328, <https://doi.org/10.1007/s10853-022-07338-x>.
- [13] J.H. Ma, N. Xu, Y.X. Luo, Y. Lin, Y.P. Pu, Enhancing the polishing efficiency of CeO₂ abrasives on the SiO₂ substrates by improving the Ce³⁺ concentration on their surface, ACS Appl. Electron. Mater. 5 (2023) 526–536, <https://doi.org/10.1021/acsaelm.2c01553526>.
- [14] K.K. Myong, J. Byun, M. Choo, H. Kim, J.Y. Kim, T. Lim, J.J. Kim, Direct and quantitative study of ceria-SiO₂ interaction depending on Ce³⁺ concentration for

- chemical mechanical planarization (CMP) cleaning, *Mater. Sci. Semicond. Process.* 122 (2021) 105500, <https://doi.org/10.1016/j.mssp.2020.105500>.
- [15] Z. Yuan, Y. He, X. Sun, Q.J.M. Wen, M. Processes, UV-TiO₂ photocatalysis-assisted chemical mechanical polishing 4H-SiC wafer, *Mater. Manuf. Process.* 33 (2018) 1214–1222, <https://doi.org/10.1080/10426914.2017.1364855>.
- [16] Y. Chen, L. Zhong, A. Chen, M. Fu, X. Lu, Highly dispersed Gd-CeO₂ nanocrystals supported on mesoporous silica composite particles towards photochemical (photo-assisted chemical) mechanical polishing, *Ceram. Int.* 49 (2023) 16932–16943, <https://doi.org/10.1016/j.ceramint.2023.02.055>.
- [17] B. Gao, W. Zhai, Q. Zhai, C. Wang, Novel photoelectrochemically combined mechanical polishing technology for scratch-free 4H-SiC surface by using CeO₂-TiO₂ composite photocatalysts and PS/CeO₂ core/shell abrasives, *Appl. Surf. Sci.* 570 (2021) 151141, <https://doi.org/10.1016/j.apsusc.2021.151141>.
- [18] B. Gao, W.J. Zhai, Q. Zhai, Y.Q. Shi, Communication—a strategy to reduce the content of residual oxide layer on SiC surface in ECM, *ECS J. Solid State Sci. Technol.* 10 (2021) 044006, <https://doi.org/10.1149/2162-8777/abf16e>.
- [19] J. Murata, Y. Ueno, K. Yodogawa, T. Sugiyama, Polymer/CeO₂-Fe₃O₄ multicomponent core-shell particles for high-efficiency magnetic-field-assisted polishing processes, *Int. J. Mach. Tool Manufact.* 101 (2016) 28–34, <https://doi.org/10.1016/j.ijmachtools.2015.11.004>.
- [20] B. Gao, W.J. Zhai, Q. Zhai, M.Z. Zhang, Novel polystyrene/CeO₂-TiO₂ multicomponent core/shell abrasives for high-efficiency and high-quality photocatalytic-assisted chemical mechanical polishing of reaction-bonded silicon carbide, *Appl. Surf. Sci.* 484 (2019) 534–541, <https://doi.org/10.1016/j.apsusc.2019.04.037>.
- [21] A. Chen, T. Wang, Y. Chen, S. Wang, Y. Chen, Development of polystyrene/polyaniline/ceria (PS/PANI/CeO₂) multi-component abrasives for photochemical mechanical polishing/planarization applications, *Appl. Surf. Sci.* 575 (2022) 151784, <https://doi.org/10.1016/j.apsusc.2021.151784>.
- [22] T. Wang, Y. Chen, A. Chen, Y. Chen, Development of carbon sphere/ceria (CS/CeO₂) hetero particles and their applications to functional abrasives toward photochemical mechanical polishing, *Appl. Surf. Sci.* 593 (2022) 153449, <https://doi.org/10.1016/j.apsusc.2022.153449>.
- [23] A. Chen, S. Wang, J. Pan, T. Wang, Y. Chen, Development of Zr- and Gd-doped porous ceria (pCeO₂) abrasives for achieving high-quality and high-efficiency oxide chemical mechanical polishing, *Ceram. Int.* 48 (2022) 14039–14049, <https://doi.org/10.1016/j.ceramint.2022.01.289>.
- [24] E. Kim, J. Lee, C. Bae, H. Seok, H.-U. Kim, T. Kim, Effects of trivalent lanthanide (La and Nd) doped ceria abrasives on chemical mechanical polishing, *Powder Technol.* 397 (2022) 117025, <https://doi.org/10.1016/j.powtec.2021.11.069>.
- [25] X. Liang, J. Xiao, B. Chen, Y. Li, Catalytically stable and active CeO₂ mesoporous spheres, *Inorg. Chem.* 49 (2010) 8188–8190, <https://doi.org/10.1021/ic100795p>.
- [26] B. Gao, W.J. Zhai, Q. Zhai, C. Wang, Novel photoelectrochemically combined mechanical polishing technology for scratch-free 4H-SiC surface by using CeO₂-TiO₂ composite photocatalysts and PS/CeO₂ core/shell abrasives, *Appl. Surf. Sci.* 570 (2021) 151141, <https://doi.org/10.1016/j.apsusc.2021.151141>.
- [27] L. Xie, J. Cheng, T. Wang, X. Lu, Mechanical wear behavior between CeO₂(100), CeO₂(110), CeO₂(111), and silicon studied through atomic force microscopy, *Tribol. Int.* 153 (2021) 106616, <https://doi.org/10.1016/j.triboint.2020.106616>.
- [28] R.C. Evans, *An Introduction to Crystal Chemistry*, The University Press, Cambridge, 1976.
- [29] B. Xu, H. Yang, Q.T. Zhang, S.S. Yuan, A. Xie, M. Zhang, T. Ohno, Design and Synthesis of Sm, Y, La and Nd-doped CeO₂ with a broom-like hierarchical structure: a photocatalyst with enhanced oxidation performance, *ChemCatChem* 12 (2020) 2638–2646, <https://doi.org/10.1002/cctc.201902309>.
- [30] A. Monshi, M.R. Foroughi, M. Monshi, Modified scherrer equation to estimate more accurately nano-crystallite size using XRD, *World J. Nano Sci. Eng.* 2 (2012) 154–160, <https://doi.org/10.4236/wjNSE.2012.23020>.
- [31] J. Tauc, R. Grigorovici, A. Vancu, Optical properties and electronic structure of amorphous germanium, *Basic Solid State Phys.* 15 (1966) 627–637, <https://doi.org/10.1002/pssb.19660150224>.
- [32] R. Maher, G. Kerherve, D. Payne, X. Yue, P. Connor, J. Irvine, L. Cohen, The reduction properties of M-doped (M=Zr, Gd) CeO₂/YSZ scaffolds Co-infiltrated with nickel, *Energy Technol.* 6 (2018) 1–9, <https://doi.org/10.1002/ente.201800146>.
- [33] A.L. Chen, Y.H. Duan, Z.Y. Mu, W.J. Cai, Y. Chen, Meso-silica/Erbium-doped ceria binary particles as functionalized abrasives for photochemical mechanical polishing (PCMP), *Appl. Surf. Sci.* 550 (2021) 149353, <https://doi.org/10.1016/j.apsusc.2021.149353>.
- [34] F. Jiang, S. Wang, B. Liu, J. Liu, L. Wang, Y. Xiao, Y. Xu, X. Liu, Insights into the influence of CeO₂ crystal facet on CO₂ hydrogenation to methanol over Pd/CeO₂ catalysts, *ACS Catal.* 10 (2020) 11493–11509, <https://doi.org/10.1021/acscatal.0c03324>.
- [35] J. Cheng, S. Huang, Y. Li, T.Q. Wang, L.L. Xie, X.C. Liu, RE (La, Nd and Yb) doped CeO₂ abrasive particles for chemical mechanical polishing of dielectric materials: experimental and computational analysis, *Appl. Surf. Sci.* 506 (2020) 144668, <https://doi.org/10.1016/j.apsusc.2019.144668>.
- [36] J. Cheng, S. Huang, X.C. Lu, Preparation of surface modified ceria nanoparticles as abrasives for the application of chemical mechanical polishing (CMP), *ECS J. Solid State Sci. Technol.* 9 (2020) 024015, <https://doi.org/10.1149/2162-8777/ab7098>.
- [37] T. Hoshino, Y. Kurata, Y. Terasaki, K. Susa, Mechanism of polishing of SiO₂ films by CeO₂ particles, *J. Non-Cryst. Solids* 283 (2001) 129–136, [https://doi.org/10.1016/S0022-3093\(01\)00364-7](https://doi.org/10.1016/S0022-3093(01)00364-7).
- [38] A. Rajendran, Y. Takahashi, M. Koyama, M. Kubo, A. Miyamoto, Tight-binding quantum chemical molecular dynamics simulation of mechano-chemical reactions during chemical-mechanical polishing process of SiO₂ surface by CeO₂ particle, *Appl. Surf. Sci.* 244 (2005) 34–38, <https://doi.org/10.1016/j.apsusc.2004.09.126>.
- [39] K.-M. Han, S.-Y. Han, S. Sahir, N.P. Yerriboina, T.-G. Kim, N. Mahadev, J.-G. Park, Contamination mechanism of ceria particles on the oxide surface after the CMP process, *ECS J. Solid State Sci. Technol.* 9 (2020) 124004, <https://doi.org/10.1149/2162-8777/abf13>.
- [40] Z. Li, L. Jin, Z. Cao, C. Zhang, X. Cao, G. Han, S. Peng, Y. Liu, Development and characterization of a novel RE³⁺ doped Core-shell CeO₂ abrasive system and its glass CMP investigations, *Appl. Surf. Sci.* 638 (2023) 158055, <https://doi.org/10.1016/j.apsusc.2023.158055>.